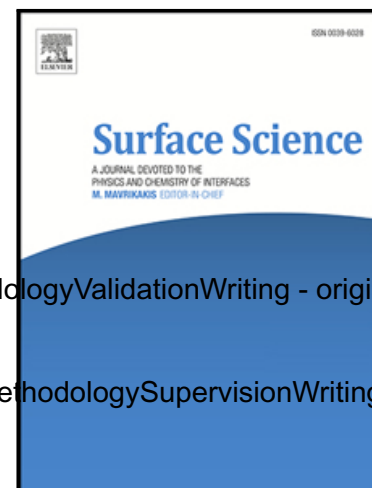


Oxidation of a c-Tb₂O₃(111) Thin Film by the Sequential Formation of Stoichiometric Phases

Christopher J. Lee ConceptualizationInvestigationFormal analysisMethodologyValidationWriting - original draftWriting - review and editing
Saumye Vashishtha InvestigationValidation ,
Ameen Sayal InvestigationValidation ,
Jason F. Weaver ConceptualizationFormal analysisFunding acquisitionMethodologySupervisionWriting - original draftWriting - review and editing

PII: S0039-6028(19)30699-5
DOI: <https://doi.org/10.1016/j.susc.2019.121555>
Reference: SUSC 121555



To appear in: *Surface Science*

Received date: 16 September 2019
Revised date: 15 November 2019
Accepted date: 10 December 2019

Please cite this article as: Christopher J. Lee ConceptualizationInvestigationFormal analysisMethodologyValidationWriting - original draftWriting - review and editing
Saumye Vashishtha InvestigationValidation ,
Ameen Sayal InvestigationValidation ,
Jason F. Weaver ConceptualizationFormal analysisFunding acquisitionMethodologySupervisionWriting - original draftWriting - review and editing
Oxidation of a c-Tb₂O₃(111) Thin Film by the Sequential Formation of Stoichiometric Phases, *Surface Science* (2019), doi: <https://doi.org/10.1016/j.susc.2019.121555>

This is a PDF file of an article that has undergone enhancements after acceptance, such as the addition of a cover page and metadata, and formatting for readability, but it is not yet the definitive version of record. This version will undergo additional copyediting, typesetting and review before it is published in its final form, but we are providing this version to give early visibility of the article. Please note that, during the production process, errors may be discovered which could affect the content, and all legal disclaimers that apply to the journal pertain.

Highlights

- Sequential development of ι -Tb₇O₁₂ and δ -Tb₁₁O₂₀ phases during c-Tb₂O₃ oxidation.
- Variable density α -TbO_x phase forms in the late stages of oxidation.
- Well-ordered ι -Tb₇O₁₂(111) structure develops after heating to 700 K.
- The δ and α phases decompose in UHV before relaxing to more stable configurations.

Oxidation of a c-Tb₂O₃(111) Thin Film by the Sequential Formation of Stoichiometric Phases

Christopher J. Lee¹, Saumye Vashishtha¹, Ameen Sayal¹, Jason F. Weaver^{1*}

¹Department of Chemical Engineering, University of Florida, Gainesville, FL 32611, USA

*To whom correspondence should be addressed, weaver@che.ufl.edu

Tel. 352-392-0869, Fax. 352-392-9513

Abstract

We used temperature-programmed desorption (TPD), low energy electron diffraction (LEED) and X-ray photoelectron spectroscopy (XPS) to investigate the oxidation of a well-ordered c-Tb₂O₃(111) thin film supported on Pt(111) by gaseous oxygen atoms in ultrahigh vacuum. Our results provide evidence that the c-Tb₂O₃ film oxidizes through the sequential development of the stoichiometric ι -Tb₇O₁₂ and δ -Tb₁₁O₂₀ phases, followed by the formation of a variable oxygen concentration α -TbO_x phase up to $x = 2$. The ι and δ -phases decompose to yield sharp O₂ TPD peaks at about 780 and 640 K, while the α -phase evolves O₂ between ~450 and 600 K during TPD. Quantitative analysis shows that changes in the XPS Tb 3d and 4d spectra caused by oxidation agree well with our estimates of the TbO_x film stoichiometry determined from TPD. We observe a well-defined LEED pattern for ι -Tb₇O₁₂(111) after heating the oxidized film to ~700 K. In contrast, several observations, including incomplete $\iota \rightarrow \delta$ conversion, lack of an observable LEED pattern for the δ -Tb₁₁O₂₀ phase, and sensitivity of α -phase formation to thermal aging of the film, indicate that the δ and α -phases develop under kinetic control for the conditions studied, such that the phases decompose in UHV at temperatures lower than those needed for these phases to stabilize into more crystalline and uniform arrangements.

Keywords: terbium oxide; oxide thin film; ceria; oxygen vacancies; oxidation

Introduction

Rare earth oxides (REOs) are widely used in applications of partial and complete oxidation catalysis due generally to their ability for oxygen storage and release [1-4]. A defining characteristic of the rare earth metals is their affinity to the formation of highly stable, irreducible sesquioxide structures, or structures of the Ln_2O_3 stoichiometry. These typically adopt the cubic fluorite-related bixbyite conformation ($\text{c-Ln}_2\text{O}_3$) in which the metal Ln assumes a trivalent +3 oxidation state within the oxide lattice. Three of the rare earth elements, Ce, Pr, and Tb, have the capability of accessing the tetravalent +4 oxidation state and forming a homologous series of well-defined, stable intermediate phases of the form $\text{Ln}_n\text{O}_{2n-2}$ ($n = 4, 6, 7, 9, 11, 12$) [5,6]. Formation of these higher oxide phases allows for additional oxygen storage and enhanced oxygen mobility necessary to facilitate redox chemistry through the Mars-van-Krevelen mechanism [7-10]. Developing an understanding of the REO redox mechanisms is challenging due to the dynamic nature of the intermediate structures and sensitivity to changes in oxidative environment.

Surface science investigations with REO thin films deposited onto crystalline metal surfaces have clarified the structural and chemical properties of REO surfaces, with ceria being the most widely studied REO film due to its prominent role in catalytic applications [9-21]. Prior studies show that $\text{CeO}_2(111)$ thin films form on hexagonally close-packed metal surfaces during Ce deposition in vacuum-level pressures of O_2 . Thermal reduction as well as reduction by molecular reagents typically generate $\text{CeO}_x(111)$ structures with randomly-distributed oxygen vacancies rather than ordered phases of intermediate stoichiometry, i.e., $1.5 < x < 2$ [12,22-24]. Over the last few years, studies have reported the formation of well-ordered, stoichiometric phases of partially-reduced ceria thin films, including $\text{c-Ce}_2\text{O}_3$, Ce_3O_5 and $\text{t-Ce}_7\text{O}_{12}$, where such phases

were generated through Ce-CeO₂ solid-state reactions [25-27] or slow reduction of CeO₂(111) [28-30]. As far as we know, however, surface science investigations of the phase evolution during the oxidation of c-Ce₂O₃(111) or other c-type REO films have not been reported.

We have previously shown that terbia films grown on Pt(111) in UHV form in the Tb₂O₃ stoichiometry and adopt a cubic fluorite (CF) (3×3) structure [31-33] rather than forming higher oxides or the c-type bixbyite structure that is favored in bulk Tb₂O₃. Highly favorable lattice matching with the Pt(111) substrate is likely responsible for the preferential formation of the (3×3) CF-Tb₂O₃(111) structure. We have also found that these CF-Tb₂O₃(111) films can be extensively oxidized at 300 K by exposure to O-atoms in UHV, but that oxidation occurs by random O-atom filling of vacancies in the CF structure without producing ordered phases at intermediate stoichiometry. More recently, we have observed that the CF-Tb₂O₃(111) film transforms to a well-ordered c-Tb₂O₃(111) structure after repeated oxidation and reduction to 1000 K in UHV, and obtained evidence that the stoichiometric ι and δ phases develop sequentially during oxidation of the c-Tb₂O₃ phase [34], analogous to the phase behavior represented in the bulk TbO_x-O₂ phase diagram [5,35,36]. Our findings suggest that vacancy-ordering in the initial c-Tb₂O₃(111) film promotes the formation of ordered, stoichiometric oxides during oxidation.

In the present study, we report that the oxidation of a c-Tb₂O₃(111) film occurs through the sequential formation of the stoichiometric ι and δ phases, followed by the development of a variable-density α -TbO_x phase. We show that a well-ordered ι -Tb₇O₁₂(111) surface structure forms after heating the oxidized film to ~700 K, but that the δ and α -phases develop under kinetic control and remain in meta-stable form for the conditions studied. Overall, our findings provide new insights for understanding the formation and reduction of stoichiometric terbia

phases, and advance strategies for preparing specific phases for fundamental studies of TbO_x surface structure and chemical reactivity.

Experimental Details

Experiments for this study were carried out in a three-level ultrahigh vacuum (UHV) chamber with a typical base pressure of 2×10^{-10} Torr. The details for this system are documented in prior studies [37-39]. Briefly, the chamber is equipped with a RF plasma source (Oxford Scientific Instruments) for generating atomic oxygen beams, a low energy electron diffraction (LEED) optics (SPECS) for characterization of surface structure, a quadrupole mass spectrometer (QMS) (Hiden) for temperature-programmed desorption (TPD) measurements, and a dual Mg/Al anode X-ray source and hemispherical analyzer (SPECS) for X-ray photoelectron spectroscopy (XPS) measurements. The plasma source is housed in a two-stage differentially-pumped beam chamber that connects to the UHV analysis chamber.

The Pt(111) crystal utilized in this study is a circular disk (10 mm x 1 mm) that was supported by tungsten wires fed through grooves located at the top and bottom edges of the crystal. The wires are held in thermal contact with a liquid nitrogen cooled copper reservoir and can be resistively heated. A type K thermocouple is spot welded to the back of the sample, and DC current supplied to the tungsten wires, regulated by a PID controller, allows for sample temperature control between the range of ~89 K to 1100 K. We cleaned the sample by sputtering the surface with 600 eV Ar^+ ions at an elevated temperature of 600 K and post annealing the sample to 1000 K. We also find that cycling the sample between 300 K and 1000 K in 5×10^{-7} Torr of O_2 is particularly effective at removing surface carbon and other adsorbed species. We

considered the sample to be clean when we observed negligible levels of carbon and oxygen in XPS (C 1s and O 1s peaks) as well as negligible amounts of CO and CO₂ evolution during TPD.

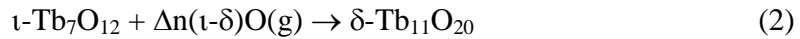
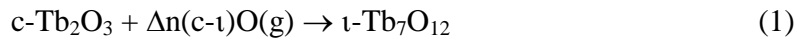
We grew terbium oxide films by the reactive physical vapor deposition (RPVD) of terbium metal (Alfa Aesar, 99.9%) onto the clean Pt(111) substrate. We vaporized Tb metal from a Ta crucible using an e-beam evaporator (McAllister Technical services) and deposited in an O₂ background of 5×10^{-7} Torr. We held the sample at 600 K during deposition followed by post annealing of the film at 1000 K in the same oxygen background. This approach has proven to be effective for improving the overall crystallinity of the initial Tb₂O₃ film [32,33,40] as well as preparing high-quality thin films of other rare earth oxides including Sm₂O₃(111) [41] and CeO₂(111) [42]. Initial terbium deposition onto Pt(111) produces a (3 × 3) CF-Tb₂O₃(111) film that we subsequently transformed to a well-defined c-Tb₂O₃(111) structure for the experiments reported in this study [33]. We discuss our recently-discovered method for the CF to bixbyite transformation in more detail below. We estimate that the average deposition rate was 0.13 ± 0.02 layer/min of Tb₂O₃. In this study, one layer is defined in reference to bulk c-type Tb₂O₃ as the O-Tb-O trilayer separation in the [111] direction. This corresponds to a height of 3.01 Å and a Tb density of 8.57×10^{14} cm⁻² per layer. We estimated film thicknesses from measurements of the attenuation of the Pt 4f XPS peak intensity. We estimate an inelastic mean free path (IMFP) of 26.9 Å for the Pt 4f photoelectrons through TbO_x using an average of the IMFP values determined from the TPP-2M and Gries equations for an electron kinetic energy of 1415 eV (see SI) [43].

We oxidized an ~18 layer c-Tb₂O₃(111) film using plasma-generated O-atom beams and investigated the oxidized films using LEED, XPS and TPD. We performed all experiments in this study using the same terbium film, and contend that the Pt substrate has a negligible influence

on the oxidation behavior due to the large thickness of the oxide film (> 5 nm). We estimate an O-atom flux of 0.018 ML s^{-1} for these experiments based on TPD measurements of oxygen uptake by Pt(111). We found that flashing the TbO_x films to 900 K and 1000 K prior to any O atom exposures was sufficient to remove surface contamination and reduce the film to a reproducible level, consistent with the Tb_2O_3 stoichiometry. After an O-atom exposure, we positioned the sample in front of a shielded mass spectrometer at a distance of ~ 5 mm and heated at a constant rate of 1 K/s until reaching a sample temperature of 1000 K. We estimate the absolute desorption yields of O_2 on the basis of O_2 TPD spectra taken after oxygen adsorption onto Pt(111). A saturation exposure to background O_2 at 300 K generates a $(2 \times 2)\text{-O}$ layer on Pt(111) with a coverage of 0.25 O-atoms per surface Pt atom. We estimate an uncertainty of about 5% in the absolute O_2 coverages based on this approach. We define 1 ML (monolayer) of O-atoms as equal to the density of Tb atoms in one O-Tb-O trilayer of $\text{TbO}_2(111)$, and report O_2 TPD yields in these units. This coverage scale provides a convenient metric for stoichiometric analysis as a single O-Tb-O trilayer of $\text{TbO}_2(111)$ (i.e., “1 layer”) contains 2 ML of O atoms and 1 ML of Tb atoms, and 0.5 ML of O-atoms are needed to completely oxidize a single trilayer of Tb_2O_3 to TbO_2 . We performed XPS measurements using non-monochromatized Al $K\alpha$ X-rays ($h\nu = 1486.6 \text{ eV}$) with the hemispherical analyzer operating in a retarding mode at a pass energy of 27 eV. We analyzed photoelectrons emitted at both 0° and 60° relative to the surface normal of the sample and averaged 20 scans for the Tb 3d and 40 scans for the Tb 4d spectra. The spectra reported here are shown as collected after a linear background subtraction and without smoothing applied.

Results

We have recently found that repeated oxidation and reduction via TPD to 1000 K transforms an initial CF-Tb₂O₃(111) film on Pt(111) to a well-ordered c-Tb₂O₃(111) structure (i.e., bixbyite), where the final film consists of nearly 10 layers of c-Tb₂O₃(111) that are separated from the Pt(111) substrate by an ~8-layer CF-Tb₂O₃(111) buffer region that likely mitigates strain in the oxide film [34]. Briefly, the bulk c-Tb₂O₃ structure is characterized by an ordered array of oxygen-vacancies, and the c-Tb₂O₃(111) surface forms a (4 × 4) structure in the CF-TbO_x(111) basis, as shown below and elaborated in the SI [33]. Our prior results further demonstrate that c-Tb₂O₃(111) oxidation occurs through the successive formation of the ι -Tb₇O₁₂ and δ -Tb₁₁O₂₀ oxides, followed by the development of small quantities of a variable oxygen-density, α -TbO_x phase in the final stages of oxidation. The ι -Tb₇O₁₂ and δ -Tb₁₁O₂₀ oxides have well-defined stoichiometry, with the structures characterized by long-range ordering of oxygen-vacancies in the lattice [44,45]. The stoichiometric coefficients of the ι -Tb₇O₁₂ and δ -Tb₁₁O₂₀ oxides are $x = 1.714$ and 1.818 , respectively, when represented as TbO_x. In contrast, the α -TbO_x phase adopts the CF-structure and can accommodate varying quantities of O-atoms up to $x = 2$. Successive formation of ι -Tb₇O₁₂ and δ -Tb₁₁O₂₀ may be described, in principle, by the following sequence of reactions,



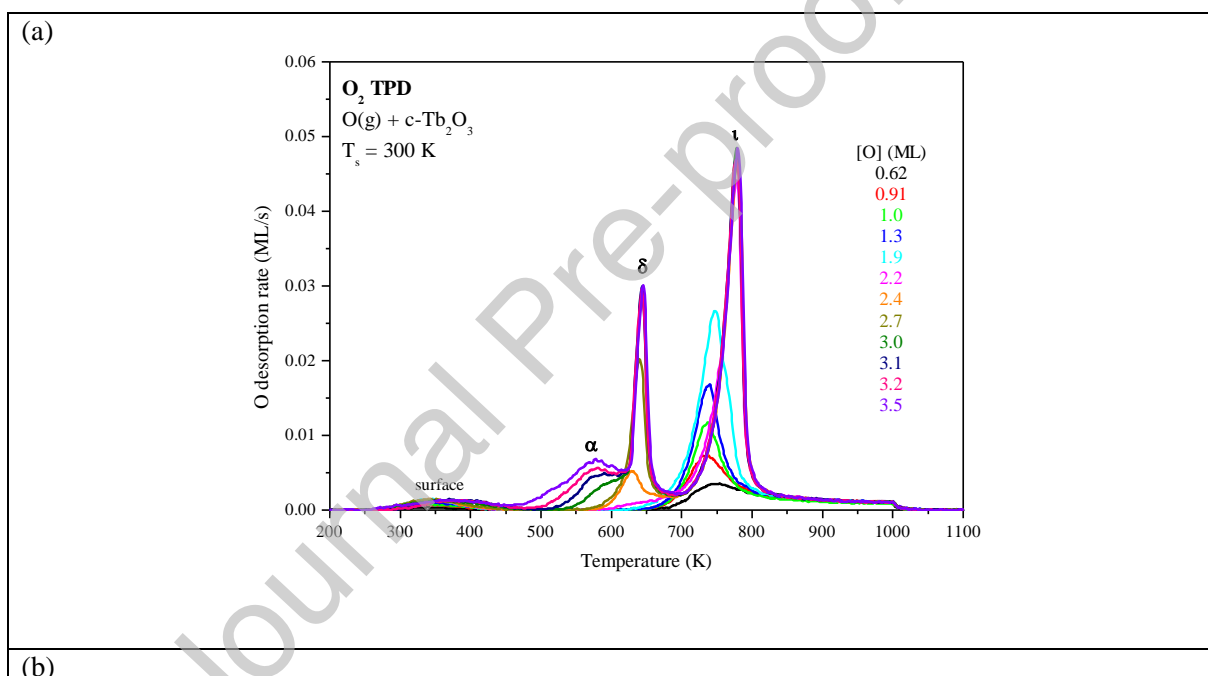
where $\Delta n(\text{c-}\iota)$ and $\Delta n(\iota\text{-}\delta)$ are equal to 0.214 ML and 0.104 ML of O-atoms per layer and we define a layer as a trilayer of the CF-TbO_x(111) structure, as mentioned in Experimental Details. Thus, oxidation of the c-Tb₂O₃ region initially follows reaction (1) and produces a mixture of the ι -Tb₇O₁₂ and c-Tb₂O₃ phases, with the volume fraction of the ι -Tb₇O₁₂ phase increasing until the

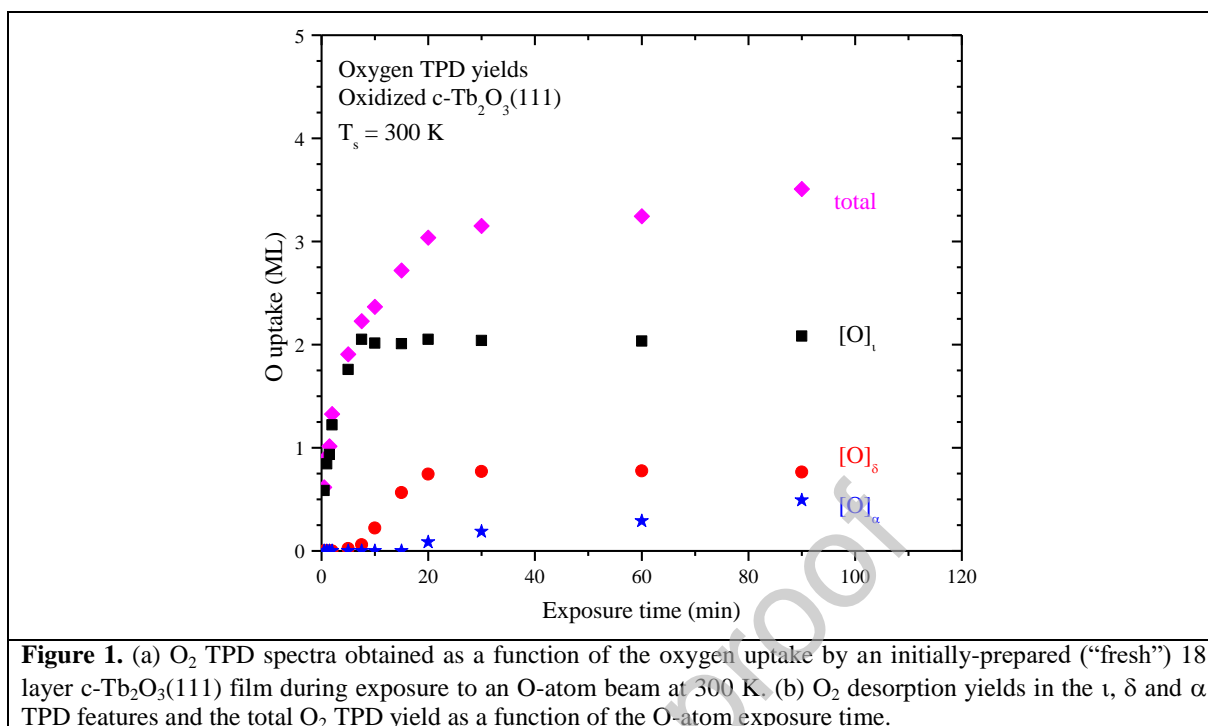
entire c-Tb₂O₃ region transforms to ι -Tb₇O₁₂ at an average stoichiometric coefficient of $x = 1.714$. Continued oxidation thereafter occurs by reaction (2) and produces a mixture of the ι -Tb₇O₁₂ and δ -Tb₁₁O₂₀ phases. Our prior work provides evidence that reaction (2) reaches only about 75% conversion before a new phase, designated as the variable O-density α -TbO_x phase, begins to form.

In our analysis of the O₂ TPD spectra [34], we compute the number of layers of the ι -phase (L_{ι}) that results from c-Tb₂O₃ oxidation using the equation, $L_{\iota} = [\text{O}]_{\iota}/\Delta n(\text{c-}\iota)$ where $[\text{O}]_{\iota}$ is the O₂ TPD yield determined for decomposition of the ι -phase. Similarly, we compute the number of layers of δ -phase using the equation $L_{\delta} = [\text{O}]_{\delta}/\Delta n(\iota\text{-}\delta)$ where $[\text{O}]_{\delta}$ is the yield of oxygen that desorbs in the δ TPD peak. Our previous work as well as the current study provide evidence that the entire c-Tb₂O₃ region oxidizes to the ι -phase prior to further oxidation, and thus that the total number of layers of c-Tb₂O₃ in the film (L) is equal to the number of layers of the ι -phase that decomposes at saturation of the ι TPD peak, i.e., $L = L_{\iota,\text{sat}}$ [34]. Finally, we define an average stoichiometric coefficient of the TbO_x film as $x = [\text{O}]_{\text{tot}}/L + 1.5$ where $[\text{O}]_{\text{tot}}$ is the total O₂ TPD yield measured when the oxidized film thermally reduces to c-Tb₂O₃ during TPD. On the basis of 5% uncertainty in the O₂ TPD yields, we estimate an uncertainty of ± 0.01 in the average stoichiometric coefficients determined for oxygen uptake less than about $x = 1.8$, and no greater than ± 0.02 for higher oxygen concentrations.

Oxidation of c-Tb₂O₃(111) at 300 K

We investigated the oxidation of a c-Tb₂O₃(111) thin film (~10 layers c-Tb₂O₃ on top of 8 layers of CF-Tb₂O₃) after first producing and apparently stabilizing this structure through repeated oxidation/reduction of an initial CF-Tb₂O₃(111) film [33,34]. Figure 1a shows a series of O₂ TPD spectra obtained as a function of the O-atom exposure to the c-Tb₂O₃(111) film at 300 K. We find that the ι , δ and α TPD features populate sequentially with increasing oxygen uptake into the c-Tb₂O₃ film, analogous to behavior observed during the repeated oxidation/reduction procedure that transformed the CF to the c-Tb₂O₃ structure [34]. The ι TPD peak first appears at ~735 K and intensifies sharply with increasing total oxygen uptake to ~2.2 ML. Also, the ι peak maximum gradually upshifts from 735 K to 748 K and a distinct shoulder at 764 K becomes evident as the oxygen uptake increases to 1.9 ML. The peak maximum then shifts abruptly to 779 K and becomes more sharp and intense when the uptake increases from 1.9 ML to 2.2 ML, which corresponds to a percent change from 85% to 100% of ι -phase saturation. We attribute the upshift in ι TPD peak temperature to enhanced stabilization of the ι -phase that results from an increase in the average ι -domain size, and thus an increase in the quantity of the ι -phase located within the bulk of the newly-formed crystallites rather than phase boundaries. The abrupt temperature upshift and intensification of the ι -peak toward the end of the ι -phase development may indicate that the ι -phase undergoes homogeneous nucleation throughout the c-Tb₂O₃ phase and that the resulting domains begin to impinge on each other only in the final stages of ι -Tb₇O₁₂ growth.





The δ and α TPD features develop sequentially after the ι -peak saturates at a total uptake of ~ 2.2 ML (Figure 1a). Initially the δ TPD peak appears at 630 K but upshifts to 643 K when this peak reaches saturation at a total oxygen uptake of 3.0 ML. The α TPD feature first appears as a shoulder on the leading edge of the δ TPD peak when the average stoichiometry of the film reaches about $x = 1.8$, and thereafter develops into a relatively broad feature with a maximum at 578 K as well as a small inflection near 515 K. The α TPD feature develops increasingly toward lower temperatures with increasing oxygen uptake, in contrast with the marked upshifts seen for the δ and ι TPD peaks. Also, the α TPD feature populates more slowly than the δ and ι TPD peaks and does not appear to saturate after the longest O-atom exposure conducted. We attribute the small, broad TPD peak centered at 370 K to oxygen that desorbs from the surface of the TbO_x film, likely from a chemisorbed state of atomic oxygen. We provide additional evidence to support this interpretation in the Supporting Information (SI). The surface TPD peak is evident

after the shortest O-atom exposure when only a small amount of ι -phase exists, and develops continuously with increasing oxygen uptake thereafter, reaching a saturation value of about 0.15 ML during oxidation at 300 K.

Figure 1b shows the ι , δ and α oxygen TPD yields as well as the total yield as a function of the O-atom exposure time during oxidation of the c-Tb₂O₃(111) film at 300 K. The total yield increases sharply with exposure in the early stages of oxidation and approaches an apparent plateau in the late oxidation region. The total uptake at 300 K increases to 3.0 ML during the first 20 minutes of oxidation, but increases by only 0.5 ML in the next 70 minutes. The data demonstrates that the ι , δ and α phases develop sequentially and that the slow uptake coincides with formation of the α -TbO_x phase. The ι -phase develops initially and saturates after a 7.5 minute O-atom exposure and the δ -phase develops during the 7.5 to 20 min exposures. We estimate that ~2 ML and 0.76 ML of oxygen desorbs from the ι and δ phases, respectively, when these phases saturate under the conditions studied. These yields are equal to about 9.5 and 7.3 layers of the ι and δ phases, respectively, equivalent to a mixture consisting of 77% δ -phase and 23% ι -phase. Desorption from the α -phase begins to occur only after formation of the δ -phase ceases at an average film stoichiometry of $x = 1.8$. The desorption yield from the α -TbO_x phase reaches 0.49 ML after the longest exposure conducted (90 min), at which point we estimate that the average film stoichiometry is equal to $x = 1.84$.

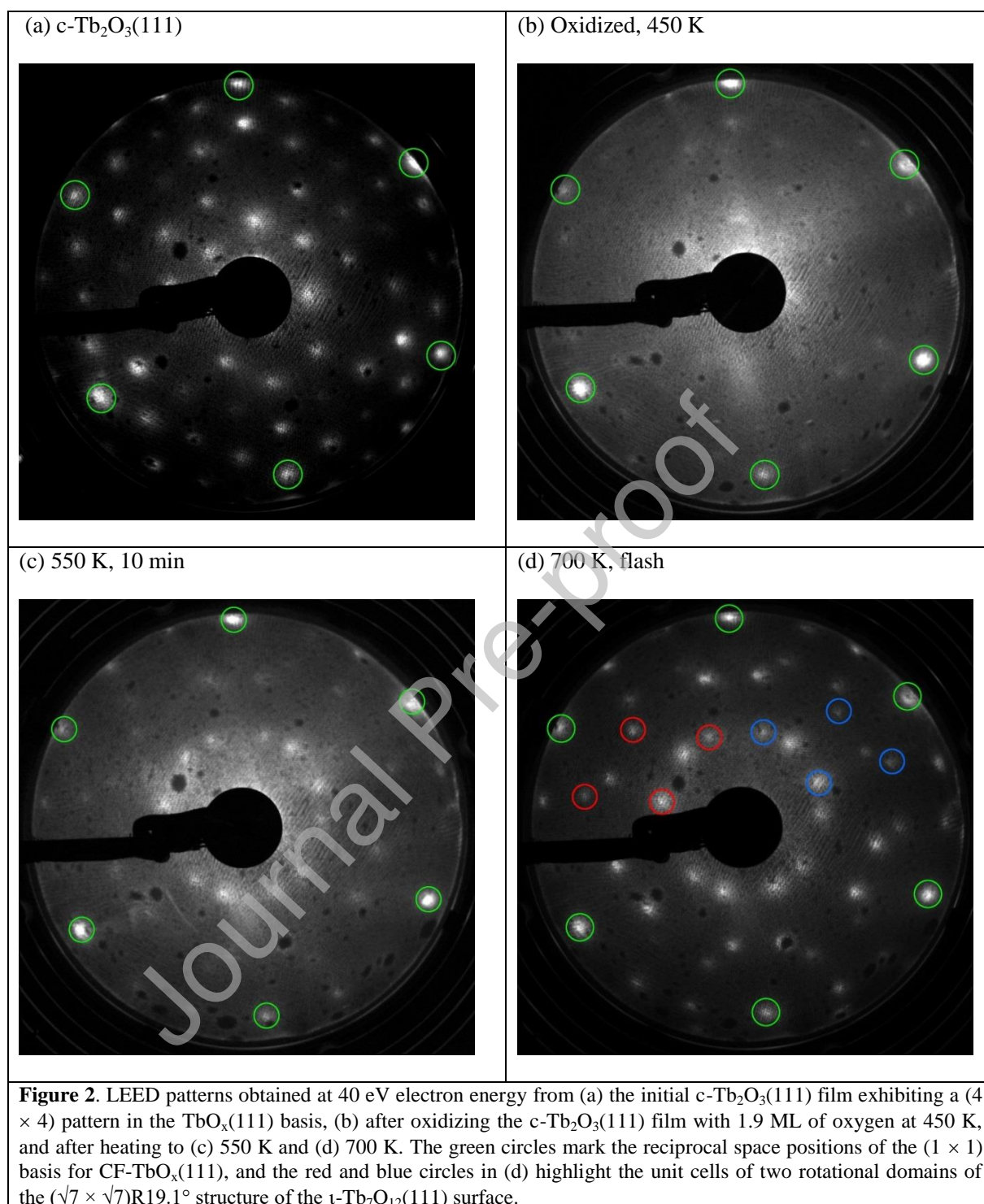
We find that the uptake curves are approximately linear, and estimate that the ι , δ and α phases form sequentially at constant rates of 0.20, 0.06 and 0.006 ML/min, respectively, prior to saturating at 300 K. The ι -phase formation rate in units of ML of O-atoms is 3.3 and 33.3 times greater than the δ and α -phase formation rates at 300 K, respectively. In terms of number of

layers, the ι and δ phases form at rates of 0.94 and 0.54 layers/min, respectively, demonstrating that the ι -phase forms more rapidly than the δ -phase at 300 K. Our results generally demonstrate that oxidation of the c-Tb₂O₃ film and transformation to the intermediate δ -Tb₁₁O₂₀ phase is facile for $x < \sim 1.8$ but that slow development of the α -phase thereafter limits further oxidation under the conditions studied. Further, we estimate that only a fraction ($\sim 77\%$) of the oxidized c-Tb₂O₃ region transforms to the δ -phase, and conclude that kinetic processes associated with vacancy-ordering limit the total amount of δ -phase that forms. Our results thus suggest kinetic limitations in the $\iota \rightarrow \delta$ oxidative transformation as the average film stoichiometry reaches $x \sim 1.8$, and slow formation of the α -TbO_x phase with increasing oxygen content thereafter.

Development of the ι -Tb₇O₁₂(111) structure with temperature

Figure 2 shows LEED patterns obtained from the initial c-Tb₂O₃(111) film, after oxidizing the film at 450 K to generate an oxygen uptake of ~ 1.9 ML, and after heating the oxidized surface to 550 K and 700 K. In these experiments, we oxidized the c-Tb₂O₃(111) film to achieve an oxygen uptake at which the ι TPD peak is nearly saturated while the δ TPD peak is negligible (Figure 1a,b). The initial c-Tb₂O₃(111) film yields a sharp (4×4) LEED pattern in the CF-TbO_x(111) basis [34], indicative of large crystalline domains (Figure 2a). After oxidizing at 450 K, the LEED image exhibits a dim (4×4) pattern and lacks discernible spots from ι -Tb₇O₁₂(111) (Figure 2b). A $(\sqrt{7} \times \sqrt{7})R19.1^\circ$ LEED pattern arising from ι -Tb₇O₁₂(111) becomes evident after

annealing for 10 min at 550 K, while the (4×4) pattern diminishes (Figure 2c). The background intensity in the LEED patterns is relatively high in the patterns observed after heating to 450 and 550 K, suggesting that domains of the ι -phase are relatively small at these conditions. The quality of the $(\sqrt{7} \times \sqrt{7})R19.1^\circ$ LEED pattern improves after flashing to 700 K as the spots become sharper and brighter and the background intensity diminishes (Figure 2d). The $(\sqrt{7} \times \sqrt{7})R19.1^\circ$ structure forms two rotational domains within the CF-TbO_x(111) basis as highlighted in Figure 2d. We note that a temperature of 550 K lies well below the ι TPD peak while 700 K is just within the leading edge of this peak. We are unable to observe a distinct LEED pattern from the δ -phase after multiple attempts to improve the crystallinity, including oxidizing within the leading edge of the δ TPD peak (600 to 630 K) as well as annealing. Instead, the measured LEED patterns only exhibit spots that are characteristic of the c-Tb₂O₃(111) or ι -Tb₇O₁₂(111) surfaces, without new spots developing that would correspond to surfaces of the δ -phase. As far as we know, the surface facets that the δ -Tb₁₁O₂₀ phase would preferentially expose have not been reported.



Our observations demonstrate that heating the oxidized film above 450 K promotes the formation of large domains of ι -Tb₇O₁₂(111) at the surface. A viable explanation is that ι -

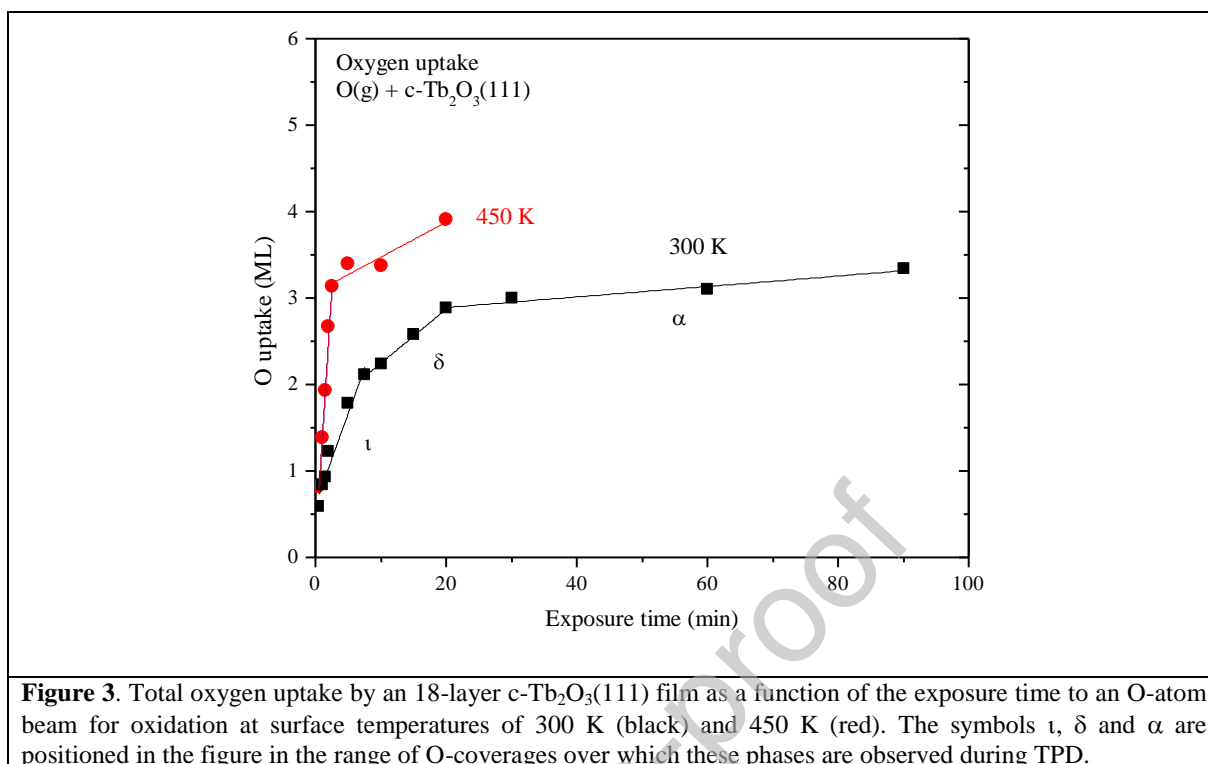
domains form at 450 K but are too small to observe with LEED. The domains then readily aggregate at higher temperature and cause the average domain size to increase, resulting in a crystalline structure that is observable with LEED. An alternate possibility is that oxidation at $T < \sim 450$ K produces a mixture of small ι -domains and a disordered TbO_x phase (α -phase), derived from random O-atom addition into the $c\text{-Tb}_2\text{O}_3$ structure, and that subsequent heating causes restructuring into large domains of crystalline $\iota\text{-Tb}_7\text{O}_{12}$. These scenarios are similar but the latter suggests that formation of the ordered $\iota\text{-Tb}_7\text{O}_{12}$ and $\delta\text{-Tb}_{11}\text{O}_{20}$ phases occurs partly during the TPD experiments.

Formation of a disordered α -phase in a fraction of the film and transformation of the disordered oxide to ordered oxides during TPD may explain why the oxidation of ι to δ fails to reach completion, apparently ceasing at a δ -phase fraction near 75%. Specifically, it is possible that oxygen desorption from the disordered α -phase becomes competitive with vacancy ordering and formation of the δ -phase at high oxygen uptake, particularly in the near-surface region of the film. As a result, oxygen desorption from the less stable α -phase could ensue before the layers near the surface can reorganize into the δ -phase structure. A LEED pattern from the δ -phase may thus be unobservable under the conditions studied because a disordered oxide is initially present in the surface layers and decomposes upon heating to the onset of δ -phase decomposition (~ 600 K). Another factor that could impede δ -phase observation with LEED is that temperatures at which the δ -phase decomposes at high rates may be needed to induce aggregation of δ -phase domains into sufficiently large crystallites. In contrast, higher stability enables the ι -phase to be heated to higher temperature than the δ -phase, thereby promoting the formation of large ι -phase domains while avoiding ι -phase decomposition. The higher stability of the ι -phase might also

promote $\alpha \rightarrow \iota$ conversion over oxygen desorption from the α -phase at the lower oxygen concentrations at which the ι -phase forms ($x < 1.714$), thus enabling oxidation of the entire c-Tb₂O₃ region to ι -Tb₇O₁₂ in our experiments.

Oxidation of c-Tb₂O₃(111) at elevated temperature

We find that the overall rate of oxidation of the c-Tb₂O₃ film increases with increasing surface temperature to 500 K and that the film continues to oxidize through the sequential formation of the ι , δ and α phases. Figure 3 compares the oxygen uptake as a function of O-atom exposure time determined from O₂ TPD measurements for c-Tb₂O₃ oxidation at 300 K and 450 K. These results show that the oxidation rate is higher at 450 K than 300 K during the formation of each of the oxide phases. For example, the δ -phase saturates within 2.5 minutes vs. 20 minutes during oxidation at 450 K vs. 300 K, reaching a total oxygen uptake of ~3 ML at each temperature. The α -phase formation rate is also higher by about a factor of six at 450 K vs. 300 K. We find that the total quantity of the ι and δ phases that form are similar (within 15%) during oxidation at 450 K vs. 300 K, indicating that the faster kinetics achieved at 450 K only marginally increases the quantity of the c-Tb₂O₃ structure that oxidizes to these phases. We did not perform the O-atom exposures for long enough time to saturate the α TPD feature at either temperature during these experiments, but find that a larger quantity of the α -phase develops in a shorter time at the higher temperature (~0.7 vs. 0.5 ML).



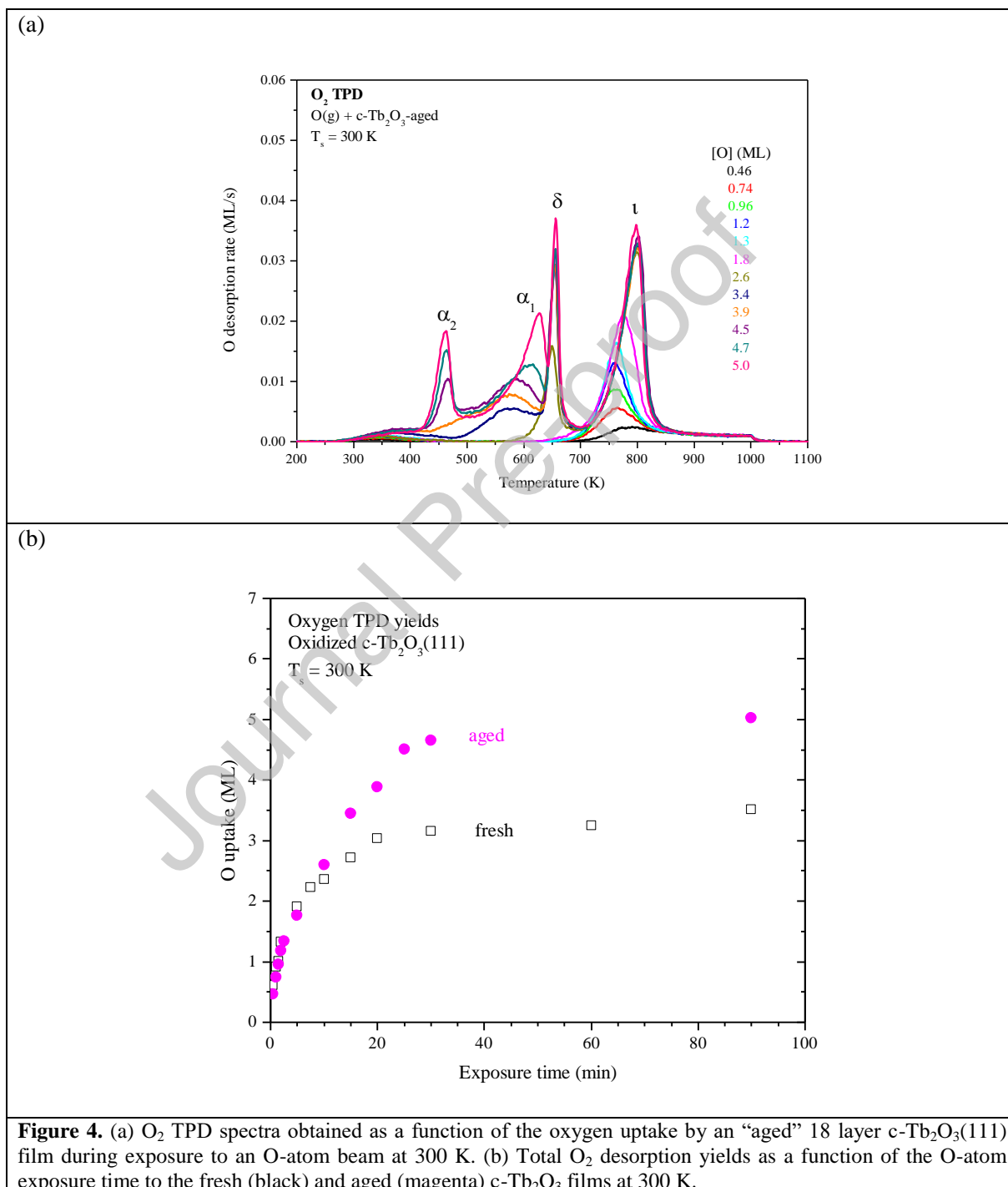
A notable feature is that the ι and δ -phase formation rates are approximately the same at 1.2 ML/min for oxidation at 450 K, whereas ι -phase formation is about three times faster than δ -phase formation at 300 K (0.2 vs. 0.06 ML/min) as seen by the abrupt decrease in the slope of the uptake curve at ~ 2 ML. We performed short uptake measurements at several temperatures and find that the corresponding temperature dependence of the ι -phase formation rate conforms well to Arrhenius behavior with an activation energy of 7.6 kJ/mol (see SI). We did not obtain sufficient data to reliably estimate kinetic parameters for δ and α -phase formation. Overall, our results demonstrate that $c-Tb_2O_3$ oxidation by O-atoms is mildly activated such that higher rates are achieved by oxidizing at temperatures above 300 K but below the onset temperature (~ 450 K) for α -phase decomposition. A key finding is that faster oxidation at 450 K causes the α -phase to develop over a time scale that is more accessible in our experiments.

Oxidation of “aged” c-Tb₂O₃(111) at 300 K

After apparently stabilizing the c-Tb₂O₃ film and investigating oxidation at 300 K (e.g., Figure 1), we investigated oxidation at several temperatures between 300 and 500 K using TPD and also performed multiple XPS and LEED experiments after oxidizing at 450 K. We found that the extent of α -phase formation at 300 K is significantly higher after we subjected the c-Tb₂O₃(111) film to these treatments. We conclude that repeatedly oxidizing the film at elevated temperature enhanced the crystallinity of the film, albeit slowly, and thereby enabled more extensive oxidation at 300 K. Hereafter, we refer to the “fresh” c-Tb₂O₃(111) film as the film that we initially synthesized from the original CF-Tb₂O₃(111) film and characterized, and the “aged”c-Tb₂O₃(111) film as the film that we investigated after repeatedly oxidizing at elevated temperature. As we show below, the film aging significantly influences the rate of α -TbO_x formation but only marginally affects ι and δ -phase formation.

Figure 4a shows a series of O₂ TPD spectra obtained as a function of the O-atom exposure to the aged c-Tb₂O₃(111) film at 300 K, and Figure 4b compares oxygen uptake curves at 300 K for the fresh and aged films. The TPD traces obtained below ~ 3 ML are similar to those obtained from the fresh film in that the ι and δ TPD peaks develop sequentially with increasing O-atom exposure. The ι and δ TPD peaks obtained from the aged film saturate at total oxygen concentrations of ~ 2.0 ML and 2.8 ML, which are similar to the saturation concentrations obtained from the fresh film (2.0 ML and 3.0 ML). The δ and ι TPD peaks appear at 655 K and 800 K at saturation of these states (Figure 4a), and are upshifted by about 12 K and 20 K, respectively, compared with our results from the fresh film (Figure 1a). We also find that the ι

TPD peak is broader for the aged vs. fresh film. The increase in the ι and δ TPD peak temperatures is consistent with the idea that larger crystalline domains of these phases develop during oxidation of the aged vs. fresh c-Tb₂O₃(111) film.



A dramatic difference between the fresh and aged films is the appearance of new and intense features in the α TPD region (~ 400 to 650 K) after oxidation of the aged c-Tb₂O₃ film. Similar to our results with the fresh film, an initially broad TPD feature (α_1) emerges at about 575 K as the total oxygen uptake increases to 3.4 ML and the δ TPD peak first becomes saturated. The α TPD features develop rapidly with further O-atom exposures to the aged film at 300 K. The α_1 TPD feature intensifies and shifts toward higher temperature with increasing oxygen uptake, eventually developing into a sharp peak at ~ 625 K. A second sharp TPD peak (α_2) at ~ 450 K appears after the total oxygen uptake exceeds about 4 ML and intensifies in parallel with the α_1 peak. Figure 4b shows that the oxidation rates are similar for the fresh and aged films as the uptake increases to ~ 3 ML during formation of the ι and δ phases, but that the uptake rate into the α -phase(s) is more than ten times greater for the aged film. As a result, the total oxygen uptake is higher in the aged vs. fresh film (5.0 vs. 3.5 ML) after the longest exposure (90 min) investigated. We estimate an average stoichiometry of $x = 2.01$ at saturation of the aged film, suggesting complete conversion of the oxidized c-Tb₂O₃(111) region to TbO₂.

Characteristics of the α_2 and α_1 TPD peaks suggest that these desorption features originate from the decomposition of ordered oxide phases. Both peaks become sharp and the α_1 peak temperature upshifts as the oxygen uptake approaches saturation. However, the approximate boundary between the α_2 and α_1 TPD features occurs at an average stoichiometry ($x \sim 1.94$) that is more oxygen-rich than any known ordered-phase of intermediate stoichiometry for bulk terbia, praseodymia or ceria [6]. According to the bulk phase diagrams, terbia as well as praseodymia and ceria should exist in the oxygen-deficient, cubic fluorite structure (α -phase) for oxygen

concentrations greater than $x = 1.833$ [36,46,47]. Researchers have reported evidence of meta-stable sub-phases in the α -PrO_x phase region, in which the α -phase structure retains memory of the ordered oxide phase (e.g., ι vs. δ) from which it formed [5,48,49]. Assigning the α_1 and α_2 TPD features to meta-stable α -phases may thus be reasonable, particularly considering that oxidation was conducted at a temperature (300 K) that is likely too low to enable full structural relaxation as discussed further below.

It is worth noting that we have been unable to observe LEED patterns that could arise from distinct intermediate structures other than ι -Tb₇O₁₂(111) (Figure 2), including after heating to various temperatures [34]. A viable explanation, however, is that the α_2 and α_1 TPD features do originate from ordered sub-phases but that they form in domains that are too small and/or remain in the subsurface of the film, and thus do not produce measurable LEED patterns. This explanation seems reasonable considering that our TPD data provides strong evidence for the formation of the δ -phase, and yet we are unable to observe a LEED pattern for the δ -structure as discussed above [5,34,45].

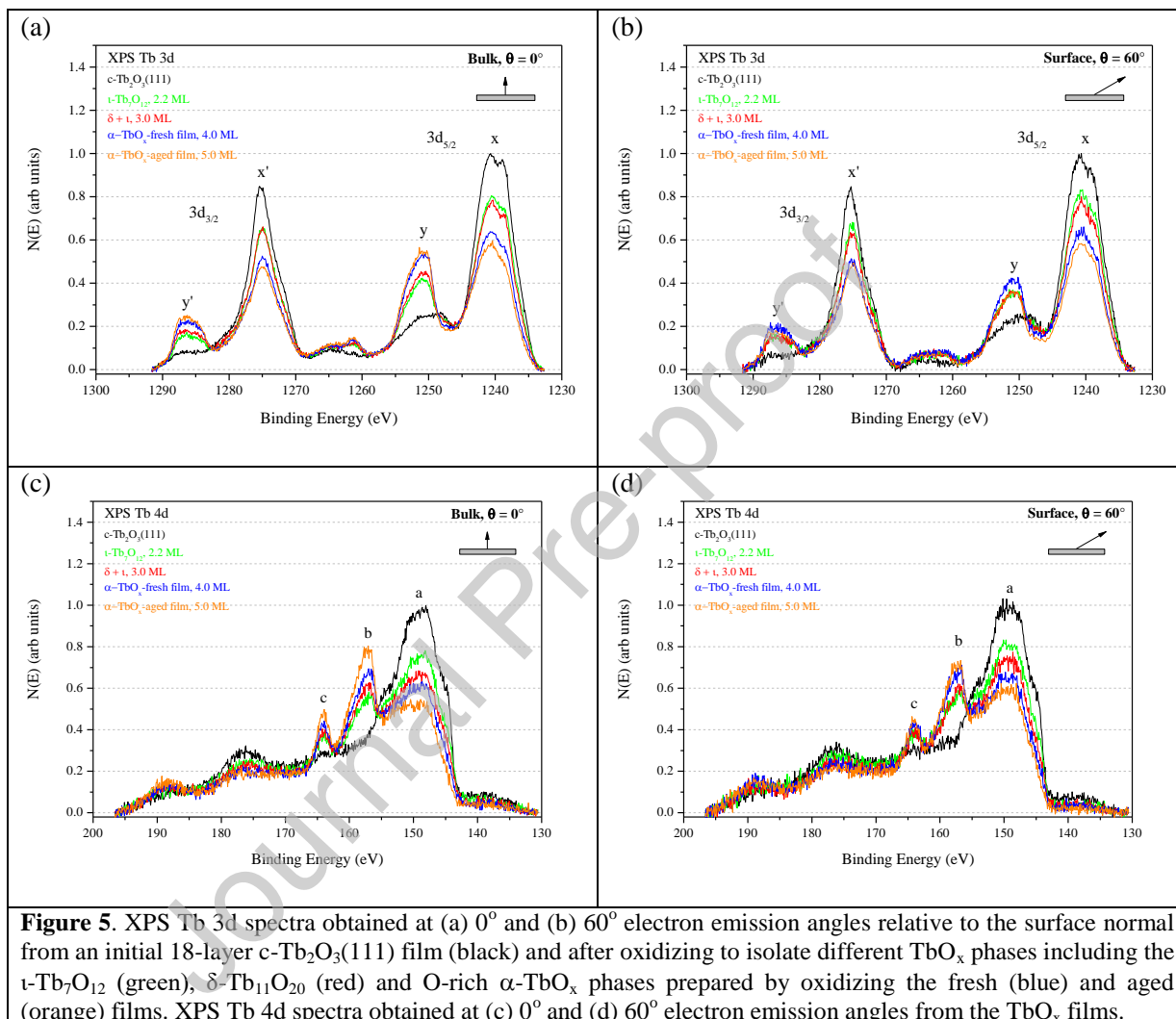
XPS characterization of oxidized c-Tb₂O₃(111)

Figures 5a and b show Tb 3d spectra obtained from the initial c-Tb₂O₃(111) film and after oxidizing to generate the oxide phases listed in the figure. We specifically generated the ι -Tb₇O₁₂ phase with 2.0 ML of oxygen by flashing to 700 K, a mixture of the δ -Tb₁₁O₂₀ + ι -Tb₇O₁₂ phases with 3.0 ML of oxygen by flashing to 600 K and the α -TbO_x phase with 4.0 ML vs. 5.0 ML after oxidizing the fresh and aged films at 300 K for 90 min. We estimate average stoichiometric coefficients of $x = 1.71, 1.80, 1.89$ and 2.03 for these oxidized films based on TPD results. We

also collected XPS data with the sample rotated at 0° and 60° relative to the analyzer to obtain information about the spatial distribution of oxide phases with respect to the vacuum-solid interface. We scaled each Tb 3d spectrum to the intensity of the Tb $3d_{5/2}$ peak obtained from the initial c-Tb₂O₃(111) film. The Tb 3d spectrum obtained from the c-Tb₂O₃(111) film exhibits dominant $3d_{5/2}$ and $3d_{3/2}$ peaks at binding energies (E_b) of 1241 and 1275 eV (x and x'), respectively, as well as small peaks (y and y') that are shifted by ~ 10 eV toward higher binding energy from the main peaks and a small feature at 1265 eV. Prior reports discuss the origins of the peaks in the Tb 3d spectra [31]. Briefly, photoemission from a Tb 3d multiplet state produces two main peaks at E_b and $\sim(E_b + 10 \text{ eV})$ that arise from different final state configurations due to mixing of the Tb 4f and O 2p states.

Figures 5a,b show that increasing the average oxidation state of the terbia film causes the main peak (x) to diminish while the secondary peak (y) concurrently intensifies, confirming prior results [31,32]. The y:x peak-height ratio, measured at the maximum peak intensities, increases by about a factor of two after oxidizing c-Tb₂O₃(111) to the ι -phase, followed by only a slight increase between the $\delta + \iota$ mixture and the ι -phase. The y:x peak ratio exhibits a larger increase ($\sim 30\text{-}45\%$) between the α -phases and the $\delta + \iota$ mixture (Figure 5a,b). The changes in y:x peak ratio with increasing oxygen uptake are qualitatively similar, but are less pronounced in the Tb 3d spectra measured at 60° vs. 0° takeoff angle. Another noticeable difference is that the y:x peak ratio is nearly the same for the α -phase of the aged vs. fresh films in the data obtained at 60° takeoff angle, but is slightly higher for the aged film at 0° takeoff angle. This difference may indicate that the additional oxygen in the aged film mainly enriches the subsurface region, resulting in a more appreciable enhancement in the Tb⁴⁺-derived peaks observed in the bulk-

sensitive (0° takeoff angle) Tb 3d spectra. We discuss quantitative analysis of the XPS spectra below.



Figures 5c and d show the Tb 4d spectra collected from the oxidized films at 0° and 60° takeoff angles, respectively. The Tb 4d spectrum obtained from the c-Tb₂O₃(111) film exhibits a main peak (a) at 149 eV as well as smaller satellite features at about 176 and 188 eV. Peaks at 157 eV (b) and 164 eV (c) intensify as the film is progressively oxidized while the main peak at

149 eV diminishes. While the changes in the Tb 4d peak intensities with increasing oxygen uptake are qualitatively similar to those seen in the Tb 3d spectra, the Tb 4d peaks derived from the Tb⁴⁺ state (peaks *b* and *c*) intensify to similar extents at 0° and 60° takeoff angle with increasing oxygen uptake (Figure 5c vs 5d). For example, the Tb⁴⁺-derived peaks in the Tb 4d spectra are noticeably larger for the α -phase generated in the aged vs. fresh film, particularly at 0° takeoff angle, whereas the intensity of the analogous Tb 3d peak (*y*) is either similar (0°) or smaller (60°) for the aged vs fresh film even though the aged film contains 20% more oxygen than the fresh film.

Our results show that the changes in the Tb 3d spectra are more sensitive to the takeoff angle than the Tb 4d spectra as the film is increasingly oxidized, exhibiting weaker intensification of the Tb⁴⁺ derived peaks at 60° takeoff angle. We attribute this difference to the higher surface sensitivity of the Tb 3d vs. 4d spectra. We estimate mean escape depths ($\lambda \cos\theta$) of 4.0 and 7.9 Å for Tb 3d photoelectrons collected at 60° and 0° takeoff angle, respectively, vs. 12.8 and 25.5 Å for Tb 4d photoelectrons measured at these angles. Given a thickness of ~3 Å for each TbO_x “layer”, the mean escape depths are equivalent to ~1.5 and 3 layers for the Tb 3d spectra and 4 and 8 layers for the Tb 4d spectra collected at 0° and 60°, respectively. These estimates show that layers deep within the ~10 layer oxidized region of the film contribute significantly to the Tb 4d photoelectron signals measured at 0° and 60° takeoff angle, whereas the near-surface layers make a larger relative contribution to the Tb 3d photoelectron yields. The weaker intensification of the Tb⁴⁺ derived peaks in the more surface sensitive Tb 3d spectra thus suggest that the oxygen concentration increases to a lesser extent in the near-surface layers of the film compared with the deeper lying layers.

Quantitative analysis of Tb core level spectra

We performed a quantitative analysis of the Tb 3d and 4d spectra to assess the extent of oxidation from measurements that probe different characteristic regions of the film below the vacuum-solid interface. Our approach is similar to that employed previously for determining the CeO_x stoichiometry from XPS Ce 3d spectra [25]. Specifically, we fit each Tb 3d and 4d spectrum with a linear combination of spectra obtained from the initial c- $\text{Tb}_2\text{O}_3(111)$ film and the aged film after extensive oxidation at 300 K. These reference films represent the most reduced and oxidized films that we studied, and have average stoichiometric coefficients of $x = 1.5$ and 2.03 , respectively, with the latter estimated from TPD data. The average stoichiometric coefficient for the aged film is slightly higher than that stated above because it includes a contribution from a small quantity of chemisorbed oxygen. We express the linear combination with the equation $y\text{Tb}_3 + (1 - y)\text{Tb}_4$, where Tb_3 and Tb_4 represent the spectra obtained from the reference Tb_2O_3 and $\text{TbO}_{2.03}$ films, and adjust the parameter y to optimize the fit to each spectrum obtained from an oxide of intermediate stoichiometry. The optimum value of y is related to an average stoichiometric coefficient from the equation $x = 1.5y + 2.03(1 - y)$. In principle, the stoichiometric coefficient determined from different core-level spectra for a given oxidized film would be the same if oxygen distributes uniformly throughout the film.

We fit spectra obtained at 0° and 60° takeoff angles using reference spectra collected only at 0° takeoff angle. We employed this approach to enable comparison of the stoichiometric coefficients determined at 0° vs. 60° takeoff angle. Also, we performed fits to normalized spectra

as well as spectra that we scaled to the intensity of the main peak obtained from c-Tb₂O₃(111). We show representative fits of the XPS spectra in the SI and note that our approach provides better agreement with the normalized Tb 3d spectra vs. scaled Tb 4d spectra. Below we report stoichiometric coefficients, $x(\text{Tb 3d})$ and $x(\text{Tb 4d})$, that are averages of the values determined from our fits to the normalized and scaled spectra in each case. These values differ by between 6% and 8% in our fits to the Tb 3d spectra obtained at 60° takeoff angle, and by less than 3% in all other spectra. We summarize the error analysis in our XPS fitting and the computed stoichiometric coefficients in the SI.

Figures 6a and b show the stoichiometric coefficients determined from the Tb 3d and 4d spectra as a function of the average stoichiometric coefficient determined from O₂ TPD data denoted as $x(\text{TPD})$. The plots include error bars determined from our analysis (see SI). The dashed line in each graph represents the relation $x(\text{XPS}) = x(\text{TPD})$ (“average line”) and includes the end points of the reference spectra obtained at 0° takeoff angle for which we set $x = 1.5$ and 2.03. Since the TPD data average the oxygen content over the entire film volume, $x(\text{XPS})$ values that lie above (below) the average line may indicate an enrichment (depletion) of oxygen within the XPS probing depth relative the average stoichiometry of the film. Figure 6a shows that the $x(\text{Tb 3d})$ values determined for $\theta = 0^\circ$ generally lie close to the TPD line, though the values determined for the $\iota + \delta$ mixture and the α -phase of the fresh film are slightly below and above the average line, respectively. While these deviations are within the error bars of the analysis, we note that a similar trend is obtained in fits to the normalized as well as the scaled Tb 3d spectra. In particular, the change in $x(\text{Tb 3d})$ with a given change in $x(\text{TPD})$ is smaller between the $\iota + \delta$ mixture and ι -phase compared with the ι -phase relative to c-Tb₂O₃, but larger between the $\iota + \delta$ mixture compared with the α -phase of the fresh film. These differences may indicate that the δ -

phase forms mainly in layers of the film that reside deeper within the characteristic Tb 3d probing depth at $\theta = 0^\circ$, while formation of the α -phase in the fresh film tends to occur closer to the vacuum-solid interface relative to the δ -phase.

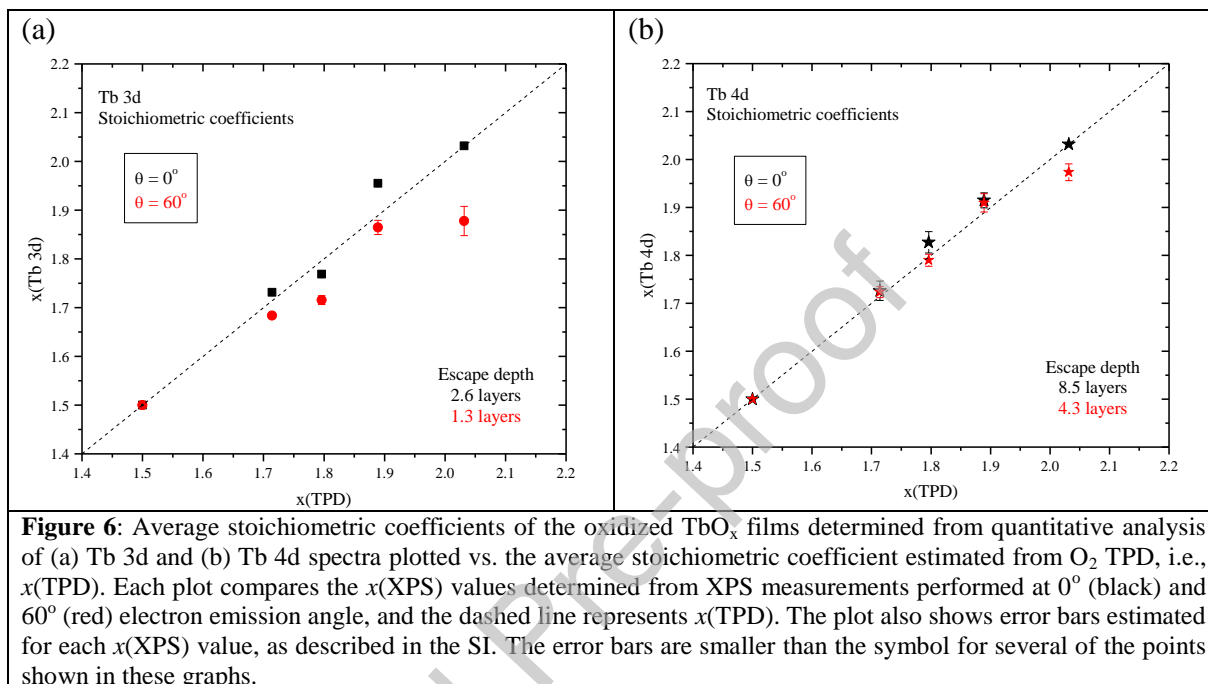


Figure 6a further shows that the $x(\text{Tb 3d})$ values are lower for Tb 3d spectra collected at $\theta = 60^\circ$ vs. 0° and that this difference increases with increasing oxygen uptake into the α -phase. This behavior suggests generally that the near-surface layers are oxygen-depleted relative to deeper-lying layers for each of the oxidized films. Considering the high surface sensitivity of the Tb 3d spectra collected at each angle, this finding may indicate that the relative oxygen-depletion is largely confined to the topmost layers of the film. The increased difference between $x(\text{Tb 3d})$ for $\theta = 60^\circ$ vs. 0° suggests an increase in the oxygen concentration gradient within the film upon formation of the α -phase, with deeper-lying layers becoming more enriched in oxygen relative to the surface.

Figure 6b shows that the $x(\text{Tb } 4d)$ values lie closer to the average line compared with the $x(\text{Tb } 3d)$ values and that the differences between $x(\text{Tb } 4d)$ values obtained at $\theta = 0^\circ$ and 60° are also smaller. Since the mean escape depths are larger for the Tb 4d photoelectrons, deeper-lying layers make a larger contribution to the Tb 4d compared with Tb 3d spectra. As a result, the $x(\text{Tb } 4d)$ values should be more representative of the stoichiometry averaged across the film and thus lie close to the average values determined from TPD, consistent with our observations. Also, deep-lying layers contribute significantly to the Tb 4d spectra collected at $\theta = 60^\circ$ due to the high Tb 4d photoelectron kinetic energy (> 1300 eV) in our measurements. For this reason, a variation in the oxygen concentration in the near-surface layers is less evident in the angle-resolved Tb 4d spectra. Overall, our analysis of the Tb 3d and 4d spectra provide evidence that the near-surface layers of the oxidized film are oxygen-depleted relative to deeper lying layers, and that the oxygen-concentration gradient becomes slightly more pronounced in the O-rich $\alpha\text{-TbO}_x$ phases in both the fresh and aged films.

O 1s spectra from oxidized c-Tb₂O₃(111)

Figures 7a, b show O 1s spectra obtained at 0° and 60° takeoff angle from the initial c-Tb₂O₃(111) film and after oxidizing to generate the oxide phases from which we obtained the Tb core level spectra discussed above. We normalized the spectra to the intensity of the main O 1s peak obtained from the c-Tb₂O₃(111) film for each set of spectra. In agreement with prior results [31], the O 1s spectrum obtained from the c-Tb₂O₃(111) film exhibits a main peak at a binding energy of 528.9 eV that shifts by 0.5-0.7 eV toward lower binding energy as the film is oxidized. The O 1s peak areas generally increase in proportion to the amount of oxygen incorporated into

the oxidized TbO_x films as determined from O_2 TPD (see SI). The area of the O 1s spectrum obtained at 0° takeoff angle from the extensively oxidized fresh $\alpha\text{-TbO}_x$ film is smaller than expected. Similar to the Tb 3d data, we find that the increase in the O 1s peaks areas with increasing oxygen content is smaller for the more surface sensitive spectra (see SI), suggesting that the oxygen concentration is slightly lower in near-surface region compared with the bulk of the oxidized films.

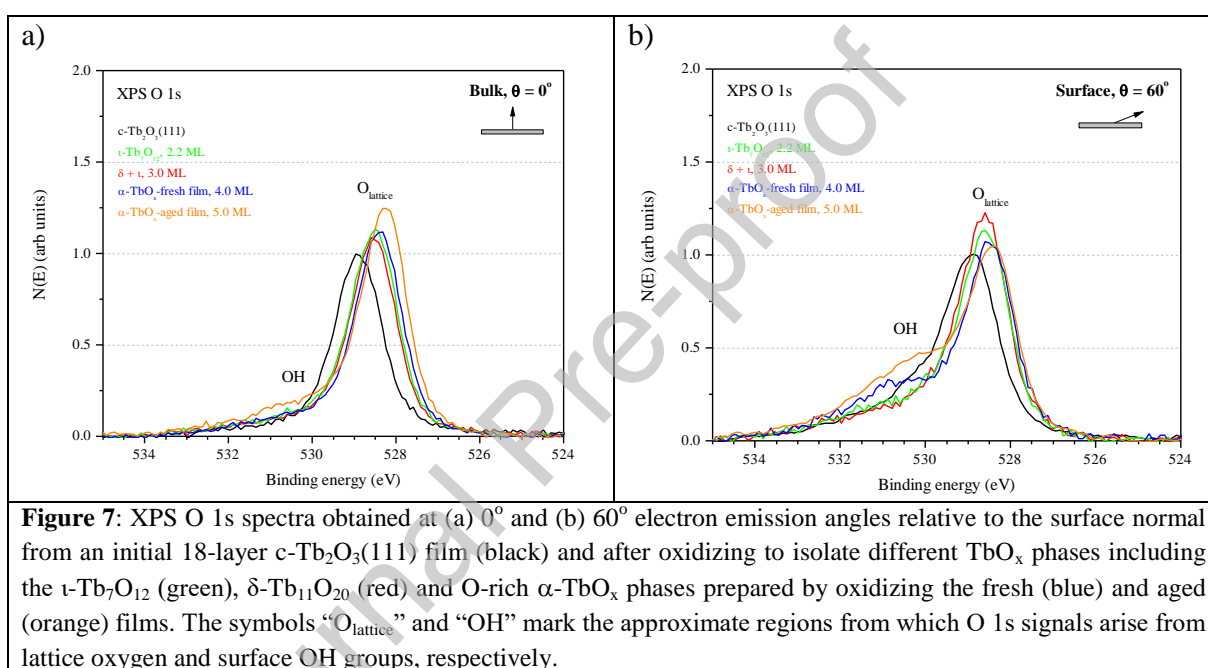


Figure 7: XPS O 1s spectra obtained at (a) 0° and (b) 60° electron emission angles relative to the surface normal from an initial 18-layer $c\text{-Tb}_2\text{O}_3(111)$ film (black) and after oxidizing to isolate different TbO_x phases including the $\alpha\text{-Tb}_7\text{O}_{12}$ (green), $\delta\text{-Tb}_{11}\text{O}_{20}$ (red) and O-rich $\alpha\text{-TbO}_x$ phases prepared by oxidizing the fresh (blue) and aged (orange) films. The symbols “O_{lattice}” and “OH” mark the approximate regions from which O 1s signals arise from lattice oxygen and surface OH groups, respectively.

The O 1s spectra further reveal the presence of OH species on the surfaces of the extensively oxidized $\alpha\text{-TbO}_x$ films and the initial $c\text{-Tb}_2\text{O}_3(111)$ film, to a lesser extent. Schaefer et al. have previously reported that OH groups form during TbO_x oxidation using a thermal oxygen cracker and yield an O 1s peak near 530.5 eV [32]. The OH species accumulate more readily on the extensively oxidized films since these surfaces were prepared at 300 K using long O-atom exposures (90 min) that liberate species such as hydrogen from the chamber walls that can adsorb on the TbO_x surface. A possibility is that the background hydrogen removes a fraction of

the oxygen from the TbO_x surfaces and/or impedes oxygen adsorption during data collection as well as oxidation of the films at 300 K, thereby causing the oxygen concentration in the near-surface region to be lower than that in the bulk. Further study is needed to characterize the adsorption and oxidation of H_2 on oxidized TbO_x surfaces to clarify the influence of H_2 on $c\text{-Tb}_2\text{O}_3(111)$ oxidation. We assert, however, that the effects are relatively minor given that we are able to oxidize the $c\text{-Tb}_2\text{O}_3(111)$ film to TbO_2 .

Discussion

Our results show that a well-ordered $c\text{-Tb}_2\text{O}_3(111)$ thin film oxidizes by the sequential development of oxide phases consistent with the stoichiometric $\iota\text{-Tb}_7\text{O}_{12}$ and $\delta\text{-Tb}_{11}\text{O}_{20}$ phases, followed by the formation of an $\alpha\text{-TbO}_x$ phase with variable oxygen concentration up to $x = 2$. In contrast, we have previously found that oxidation of an oxygen-deficient $\text{CF-Tb}_2\text{O}_3(111)$ thin film at 300 K causes the oxygen-content of the film to continuously increase, without producing the ordered ι and δ phases at intermediate stoichiometries [31]. This contrasting behavior suggests that the high-degree of vacancy ordering within the initial $c\text{-Tb}_2\text{O}_3$ phase acts to promote formation of the stoichiometric ι and δ phases for the oxidation conditions studied. We speculate that the ordered sub-lattice of vacancies in $c\text{-Tb}_2\text{O}_3$ facilitates bulk oxygen diffusion as well as the nucleation and growth of new ordered arrays of vacancies associated with the ι -phase and subsequently with the $\iota \rightarrow \delta$ conversion.

Although initial vacancy ordering promotes the formation of the ι and δ phases during oxidation, our results provide evidence that kinetic factors prevent the newly-formed oxide phases from equilibrating at the oxidation temperatures studied (300 to 450 K). Heating (e.g.,

during TPD) to near the onset of decomposition (~ 700 K) is effective for stabilizing large crystallites of the ι -phase. We assert, however, that the δ -phase begins to decompose at temperatures (~ 600 K) lower than those needed for this phase to more fully develop within the film due to kinetic barriers associated with structural rearrangements involved in the formation and growth of δ -phase domains. Supporting evidence for our interpretation is first that the rate of oxidation increases markedly with increasing oxidation temperature from 300 to 500 K, with the rate of δ and α -phase formation increasing more sharply with temperature compared with the ι -phase (Figure 2). Also, LEED shows that large crystalline domains of the ι -Tb₇O₁₂(111) structure develop only after heating above ~ 550 K, with the domains becoming larger after reaching 700 K, thus demonstrating that the ι -phase stabilizes during heating/TPD. The lack of an observable LEED pattern for the δ -Tb₁₁O₂₀ structure suggests that kinetic factors prevent the δ -phase domains from agglomerating into large crystalline domains and generating a more stable morphology at temperatures below the onset for δ -phase decomposition in UHV ($< \sim 600$ K).

Our results also show that the ι -phase fails to completely transform to the δ -phase prior to α -phase formation and that development of the α -phase is sensitive to thermal aging of the TbO_x film; both observations signal that kinetics plays a decisive role in determining the evolution of these less stable, oxide phases. Our analysis of the O₂ TPD yields indicates that the ι -phase initially converts only to the δ -phase, but that this reaction ceases after $\sim 75\%$ conversion and that further oxidation produces the α -phase instead. We estimate that the α -phase begins to form once the equivalent of 2-3 layers of the ι -phase remains within the film. This behavior represents a deviation from equilibrium since the $\iota \rightarrow \delta$ conversion should reach completion before the α -TbO_x phase begins to form at an oxygen content above $x = 1.818$ according to the TbO_x-O₂ phase

diagram [36]. We conclude that kinetic factors impede δ -phase formation once the oxygen content or quantity of δ -phase domains becomes sufficiently large. A possibility is that kinetics hinders δ -phase formation near the vacuum-solid interface and that once the δ -phase develops to a sufficient extent within the sub-surface, the random filling of residual vacancies produces a near-surface α -TbO_x phase which is favored at the conditions studied. Our angle-resolved XPS data indirectly supports this idea; however, further work is needed to characterize the oxide spatial distribution. A key finding is that kinetic factors prevent the $\iota \rightarrow \delta$ reaction from going to completion under the conditions studied.

The dramatic enhancement in the extent of α -TbO_x formation with sample “aging” provides further evidence of kinetic control in the oxidation of the film. Recall that we initially observed slow formation of the α -TbO_x phase, but that the formation rate increased by about tenfold after subjecting the film to multiple oxidation treatments at temperatures above ~ 450 K (Figure 4). This change occurred over a long time-scale and is difficult to quantify as result. We note that the film aging negligibly affected the ι and δ -phase formation rates. We speculate that gradual ripening of the c-Tb₂O₃ crystalline domains occurred during film aging and is responsible for the enhanced development of the α -TbO_x phase that we observe, implying that oxygen incorporation into the film becomes more facile when the characteristic crystalline domain size increases. We have recently reported similar behavior during the redox-induced transformation of CF to c-Tb₂O₃(111) in that the c-Tb₂O₃ phase becomes increasingly oxidized during exposure to O-atoms as the quantity of c-Tb₂O₃ phase generated and thus the characteristic domain size of this phase increases [34]. Lastly, the appearance of distinct O₂ TPD peaks in the α -phase decomposition region is further indicative of the α -phase forming under kinetically-controlled conditions since

this behavior suggests that the α -phase(s) retain memory of the phases from which they formed, i.e., the ι vs. δ -phases, as opposed to the entire film transforming into a relaxed CF-TbO₂ structure.

Our results provide information that can guide the preparation of distinct TbO_x phases for further characterization of the oxide structures as well as surface chemical reactivity. Our results suggest that oxidation at elevated temperature and oxygen chemical potential (e.g., elevated O₂ pressure) is needed to overcome kinetic barriers and generate more uniform and stable morphologies of the δ and α -phases, e.g., larger crystalline domains of the δ -phase. We emphasize that O₂ TPD has been essential for identifying and characterizing the evolution of oxide phases during Tb₂O₃ oxidation since the various oxides exhibit significant differences in thermal stability and formation kinetics. Additional structural and compositional characterization is needed to further advance the understanding of the oxide phase development in these TbO_x thin films. Our results suggest that such characterization will benefit greatly from an ability to achieve spatial resolution throughout the film, and distinguish surface from bulk structures.

Summary

We investigated the oxidation of a well-ordered c-Tb₂O₃(111) thin film by gaseous O-atoms in UHV using TPD, LEED and XPS. Our results show that oxidation occurs through the sequential development of the stoichiometric ι -Tb₇O₁₂ and δ -Tb₁₁O₂₀ phases, followed by the formation of an α -TbO_x phase with variable oxygen concentration up to $x = 2$. We find that the ι and δ phases decompose to yield sharp O₂ TPD peaks at about 780 and 640 K, respectively, while the α -TbO_x phase liberates O₂ between about 400 and 650 K during TPD. We further demonstrate that

changes in the XPS Tb 3d and 4d spectra caused by oxidation agree well with the oxygen stoichiometry determined from O₂ TPD. We find that heating to ~700 K generates a highly crystalline ι -Tb₇O₁₂(111) surface structure, whereas several observations indicate that the α and δ -phases form under kinetic control, including incomplete $\iota \rightarrow \delta$ conversion, lack of an observable LEED pattern for the δ -phase and sensitivity of α -phase formation to thermal aging of the c-Tb₂O₃ film. Our results suggest that the α and δ -phases decompose in UHV at temperatures lower than those needed for these phases to more closely approach equilibrium arrangements. Our study provides insights for understanding the oxidation of a c-Tb₂O₃(111) film and methods for generating the stoichiometric ι and δ -phases for model studies of terbia surface structure and chemical reactivity.

Supporting Information

Inelastic mean free path parameters to determine CF-Tb₂O₃(111) film thickness; Structural models of cubic fluorite and bixbyite TbO_x; Temperature dependence of the ι -phase formation rate and Arrhenius analysis; Deconvolution of XPS Tb 3d and 4d spectra obtained from oxidized c-Tb₂O₃ films; Oxygen adsorption on c-Tb₂O₃(111) at low temperature; Average stoichiometric coefficients determined from O 1s spectra.

Author Statement

Christopher J. Lee: Conceptualization; Investigation; Formal analysis; Methodology; Validation; Writing - original draft; Writing – review & editing. **Saumye Vashishtha:** Investigation; Validation. **Ameen Sayal:** Investigation; Validation. **Jason F. Weaver:** Conceptualization; Formal analysis; Funding acquisition; Methodology; Supervision; Writing - original draft; Writing – review & editing.

Declaration of competing interests

The authors have no interests to declare.

Acknowledgements

We gratefully acknowledge financial support for this work provided by the National Science Foundation, Division of Chemistry through grant number 1464765.

References

- [1] A.G. Dedov, A.S. Loktev, I.I. Moiseev, A. Aboukais, J.F. Lamonier, I.N. Filimonov, Oxidative coupling of methane catalyzed by rare earth oxides: Unexpected synergistic effect of the oxide mixtures, *Appl. Catal., A*, 245 (2003) 209-220.
- [2] K. Asami, K.-i. Kusakabe, N. Ashi, Y. Ohtsuka, Synthesis of ethane and ethylene from methane and carbon dioxide over praseodymium oxide catalysts, *Appl. Catal., A*, 156 (1997) 43-56.
- [3] O. Forlani, S. Rossini, Rare earths as catalysts for the oxidative coupling of methane to ethylene, *Mater. Chem. Phys.*, 31 (1992) 155-158.
- [4] K. Otsuka, K. Jinno, A. Morikawa, The catalysts active and selective in oxidative coupling of methane, *Chem. Lett.*, 14 (1985) 499-500.
- [5] G.-y. Adachi, N. Imanaka, The Binary Rare Earth Oxides, *Chem. Rev.*, 98 (1998) 1479-1514.
- [6] P. Kunzmann, L. Eyring, On the crystal structures of the fluorite-related intermediate rare-earth oxides, *J. Solid State Chem.*, 14 (1975) 229-237.
- [7] Y. Takasu, T. Yoko-o, M. Matsui, Y. Matsuda, I. Toyoshima, Catalytic reactivity of the lattice oxygen atoms of terbium oxide, *J. Catal.*, 77 (1982) 485-490.
- [8] A. Trovarelli, Catalytic Properties of Ceria and CeO₂-Containing Materials, *Catalysis Reviews*, 38 (1996) 439-520.
- [9] D.R. Mullins, The surface chemistry of cerium oxide, *Surf. Sci. Rep.*, 70 (2015) 42-85.
- [10] Z.C. Kang, L. Eyring, Lattice Oxygen Transfer in Fluorite-Type Oxides Containing Ce, Pr, and/or Tb, *J. Solid State Chem.*, 155 (2000) 129-137.
- [11] D.R. Mullins, P.V. Radulovic, S.H. Overbury, Ordered cerium oxide thin films grown on Ru(0001) and Ni(111), *Surf Sci.*, 429 (1999) 186-198.
- [12] M. Alexandrou, R.M. Nix, The growth, structure and stability of ceria overlayers on Pd(111), *Surf Sci.*, 321 (1994) 47-57.
- [13] C. Hardacre, G.M. Roe, R.M. Lambert, Structure, composition and thermal properties of cerium oxide films on platinum {111}, *Surf Sci.*, 326 (1995) 1-10.
- [14] K.-D. Schierbaum, Ordered ultra-thin cerium oxide overlayers on Pt(111) single crystal surfaces studied by LEED and XPS, *Surf Sci.*, 399 (1998) 29-38.
- [15] S. Eck, C. Castellarin-Cudia, S. Surnev, M.G. Ramsey, F.P. Netzer, Growth and thermal properties of ultrathin cerium oxide layers on Rh(111), *Surf Sci.*, 520 (2002) 173-185.
- [16] F. Esch, S. Fabris, L. Zhou, T. Montini, C. Africh, P. Fornasiero, G. Comelli, R. Rosei, Electron Localization Determines Defect Formation on Ceria Substrates, *Science*, 309 (2005) 752.
- [17] M. Engelhard, S. Azad, C.H.F. Peden, S. Thevuthasan, X-ray Photoelectron Spectroscopy Studies of Oxidized and Reduced CeO₂(111) Surfaces, *Surf. Sci. Spectra*, 11 (2004) 73-81.
- [18] V. Matolín, J. Libra, I. Matolínová, V. Nehasil, L. Sedláček, F. Šutara, Growth of ultra-thin cerium oxide layers on Cu(111), *Appl. Surf. Sci.*, 254 (2007) 153-155.
- [19] S. Torbrugge, M. Reichling, A. Ishiyama, S. Morita, O. Custance, Evidence of subsurface oxygen vacancy ordering on reduced CeO₂(111), *Phys. Rev. Lett.*, 99 (2007) 056101.
- [20] J. Graciani, K. Mudiyanse, F. Xu, A.E. Baber, J. Evans, S.D. Senanayake, D.J. Stacchiola, P. Liu, J. Hrbek, J.F. Sanz, J.A. Rodriguez, Highly active copper-ceria and copper-ceria-titania catalysts for methanol synthesis from CO₂, *Science*, 345 (2014) 546-550.
- [21] A. Schaefer, B. Hagman, J. Höcker, U. Hejral, J.I. Flege, J. Gustafson, Thermal reduction of ceria nanostructures on rhodium(111) and re-oxidation by CO₂, *Phys. Chem. Chem. Phys.*, 20 (2018) 19447-19457.
- [22] T. Duchoň, J. Hackl, J. Höcker, K. Veltruská, V. Matolín, J. Falta, S. Cramm, S. Nemšák, C. Schneider, J. Flege, S. Senanayake, Exploiting Micro-Scale Structural and Chemical Observations in Real Time for Understanding Chemical Conversion: LEEM/PEEM Studies over CeO_x-Cu(111), *Ultramicroscopy*, 183 (2017) 84-88.
- [23] L.H. Chan, J. Yuhara, Growth and structure of ultrathin cerium oxide films on Rh(111), *J. Chem. Phys.*, 143 (2015) 074708.

- [24] G. Gasperi, L. Amidani, F. Benedetti, F. Boscherini, P. Glatzel, S. Valeri, P. Luches, Electronic properties of epitaxial cerium oxide films during controlled reduction and oxidation studied by resonant inelastic X-ray scattering, *Phys. Chem. Chem. Phys.*, 18 (2016) 20511-20517.
- [25] T. Skála, F. Šutara, K.C. Prince, V. Matolín, Cerium oxide stoichiometry alteration via Sn deposition: Influence of temperature, *J. Electron. Spectrosc. Relat. Phenom.*, 169 (2009) 20-25.
- [26] V. Stetsovych, F. Pagliuca, F. Dvorak, T. Duchon, M. Vorokhta, M. Aulicka, J. Lachnitt, S. Schernich, I. Matolinova, K. Veltruska, T. Skala, D. Mazur, J. Myslivecek, J. Libuda, V. Matolin, Epitaxial Cubic Ce₂O₃ Films via Ce-CeO₂ Interfacial Reaction, *J Phys Chem Lett*, 4 (2013) 866-871.
- [27] T. Duchoň, F. Dvořák, M. Aulická, V. Stetsovych, M. Vorokhta, D. Mazur, K. Veltruská, T. Skála, J. Mysliveček, I. Matolínová, V. Matolín, Ordered Phases of Reduced Ceria As Epitaxial Films on Cu(111), *J. Phys. Chem. C*, 118 (2014) 357-365.
- [28] H. Wilkens, O. Schuckmann, R. Oelke, S. Gevers, A. Schaefer, M. Bäumer, M.H. Zoellner, T. Schroeder, J. Wollschläger, Stabilization of the ceria 1-phase (Ce₇O₁₂) surface on Si(111), *Appl. Phys. Lett.*, 102 (2013) 111602.
- [29] H. Wilkens, O. Schuckmann, R. Oelke, S. Gevers, M. Reichling, A. Schaefer, M. Bäumer, M.H. Zoellner, G. Niu, T. Schroeder, J. Wollschläger, Structural transitions of epitaxial ceria films on Si(111), *Phys. Chem. Chem. Phys.*, 15 (2013) 18589-18599.
- [30] R. Olbrich, G.E. Murgida, V. Ferrari, C. Barth, A.M. Llois, M. Reichling, M.V. Ganduglia-Pirovano, Surface Stabilizes Ceria in Unexpected Stoichiometry, *J. Phys. Chem. C*, 121 (2017) 6844-6851.
- [31] W. Cartas, R. Rai, A. Sathe, A. Schaefer, J.F. Weaver, Oxidation of a Tb₂O₃(111) Thin Film on Pt(111) by Gas-Phase Oxygen Atoms, *J. Phys. Chem. C*, 118 (2014) 20916-20926.
- [32] A. Schaefer, W. Cartas, R. Rai, M. Shipilin, L.R. Merte, E. Lundgren, J.F. Weaver, Methanol Adsorption and Oxidation on Reduced and Oxidized TbO_x(111) Surfaces, *J. Phys. Chem. C*, 120 (2016) 28617-28629.
- [33] C. Lee, V. Mehar, J.F. Weaver, Growth and Structure of Tb₂O₃(111) Films on Pt(111), *J. Phys. Chem. C*, 122 (2018) 9997-10005.
- [34] C.J. Lee, A. Sayal, S. Vashishtha, J.F. Weaver, Redox-Mediated Transformation of a Tb₂O₃(111) Thin Film from the Cubic Fluorite to Bixbyite Structure, Submitted, (2019).
- [35] H. Inaba, A. Navrotsky, L. Eyring, Thermochemical study of the phase reaction TbO_{1.5+x} + (3/28 - x/2) O₂ --> (1/7)Tb₇O₁₂, *J. Solid State Chem.*, 37 (1981) 77-84.
- [36] L. Eyring, The Binary Lanthanide Oxides: Synthesis and Identification, in: G. Meyer, L.R. Morss (Eds.) *Synthesis of Lanthanide and Actinide Compounds*, Springer Netherlands, Dordrecht, 1991, pp. 187-224.
- [37] H.H. Kan, R.B. Shumbera, J.F. Weaver, Hot precursor reactions during the collisions of gas-phase oxygen atoms with deuterium chemisorbed on Pt(100), *J. Chem. Phys.*, 126 (2007) 134704.
- [38] R. Bradley Shumbera, H.H. Kan, J.F. Weaver, The transition from surface to bulk oxide growth on Pt(100): Precursor-mediated kinetics, *Surf Sci.*, 601 (2007) 4809-4816.
- [39] A.L. Gerrard, J.-J. Chen, J.F. Weaver, Oxidation of Nitrided Si(100) by Gaseous Atomic and Molecular Oxygen, *J. Phys. Chem. B*, 109 (2005) 8017-8028.
- [40] J. Höcker, W. Cartas, A. Schaefer, M. Bäumer, J.F. Weaver, J. Falta, J.I. Flege, Growth, Structure, and Stability of the High-Index TbO_x(112) Surface on Cu(111), *J. Phys. Chem. C*, 119 (2015) 14175-14184.
- [41] J.-H. Jhang, A. Schaefer, W. Cartas, S. Epuri, M. Bäumer, J.F. Weaver, Growth and Partial Reduction of Sm₂O₃(111) Thin Films on Pt(111): Evidence for the Formation of SmO(100), *J. Phys. Chem. C*, 117 (2013) 21396-21406.
- [42] W. Xiao, Q. Guo, E.G. Wang, Transformation of CeO₂(111) to Ce₂O₃(0001) films, *Chem. Phys. Lett.*, 368 (2003) 527-531.
- [43] C.J. Powell, A. Jablonski, NIST Electron Inelastic-Mean-Free-Path Database, in, National Institute of Standards and Technology, Gaithersburg, Maryland 20899, 2010.
- [44] J. Zhang, R.B. Von Dreele, L. Eyring, The Structures of Tb₇O₁₂ and Tb₁₁O₂₀, *J. Solid State Chem.*, 104 (1993) 21-32.

- [45] R.T. Tuenge, L. Eyring, Structures of the intermediate phases in the terbium oxide system, *J. Solid State Chem.*; (United States), (1982) 75-89.
- [46] S. Gevers, T. Weisemoeller, A. Schaefer, V. Zielasek, M. Bäumer, J. Wollschläger, Structure of oxygen-plasma-treated ultrathin praseodymia films on Si(111), *Phys. Rev. B*, 83 (2011).
- [47] O. Kuschel, F. Dieck, H. Wilkens, S. Gevers, J. Rodewald, C. Otte, M.H. Zoellner, G. Niu, T. Schroeder, J. Wollschläger, Plasma Enhanced Complete Oxidation of Ultrathin Epitaxial Praseodymia Films on Si(111), *Materials (Basel)*, 8 (2015) 6379-6390.
- [48] F.J. Lincoln, J.R. Sellar, B.G. Hyde, A new examination of the thermodynamic properties of the oxygen-deficient fluorite-type phase $\alpha\text{-PrO}_2\text{-}\delta$, *J. Solid State Chem.*, 74 (1988) 268-276.
- [49] M.S. Jenkins, R.P. Turcott, L. Eyring, in: *The Chemistry of Extended Defects in Non-metallic Crystals*, North-Holland Publishing Company, Amsterdam, 1970, pp. 36-53.

Graphical Abstract

